LHCB 98-002 TRIG/MUON

The LHCb Level 0 Muon Trigger

M. Borkovsky[2], G. Corti[1], B. Cox[1], A. Tsaregorodtsev[2], K. Nelson[1], A. Vorobyov[2]

1) University of Virginia
2) Petersburg Nuclear Physics Institute

Abstract

The LHCb Level 0 high p_t muon trigger strategy and performance are discussed and the components of the muon detector necessary for the L0 trigger are described. The Level 0 trigger algorithm necessary to achieve the desired suppression of triggers due to $\pi/K \rightarrow \mu$ decays in minimum bias events while maintaining good efficiency for semimuononic B decays is described. Results of various studies of the effect of variation of detector parameters on this trigger are presented.

Contents

List of Figures

List of Tables

1 Introduction

The components of the LHCb Muon Detector which participate in the LHCb L0 muon trigger are schematically shown in Fig. 1.

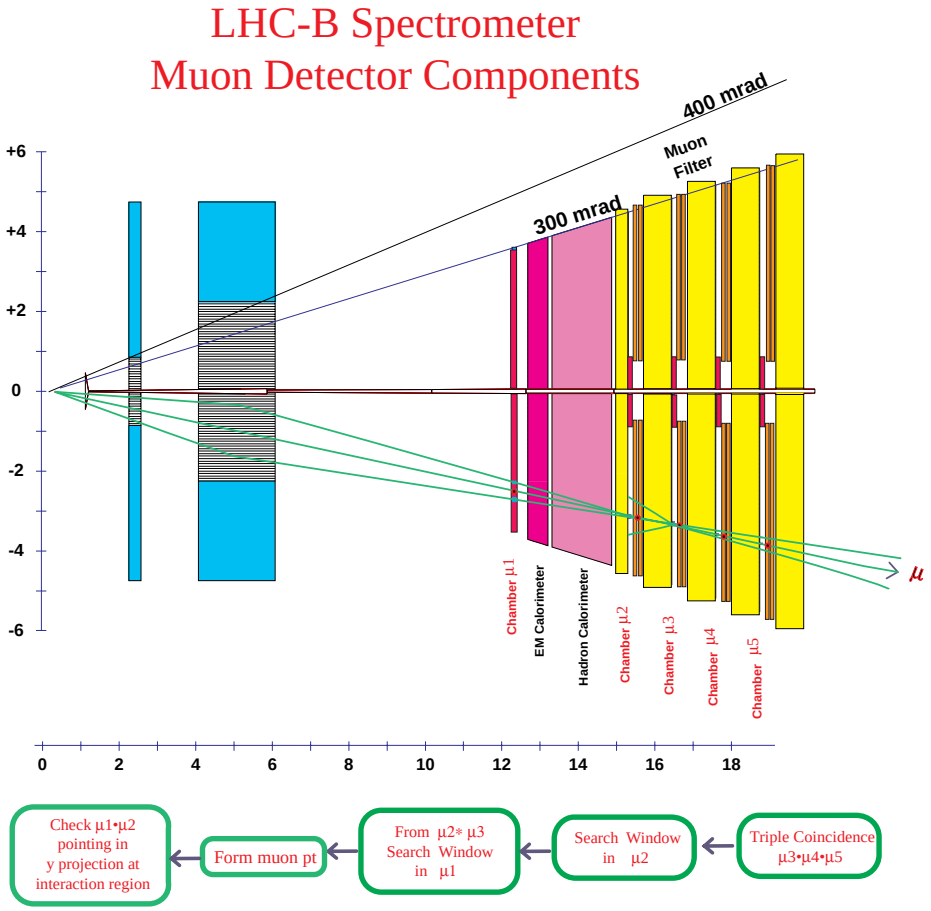

Figure 1: Schematic of Muon System components and trigger algorithm

As can be seen, the muon detector is composed of a shield to attenuate hadrons, photons and electrons. The components of the shield are the electromagnetic and hadronic calorimeter and five layers of steel as described in Table 1. The five muon stations μ1, 2 ,3 4 and 5 shown in Fig. 1 incorporate either Cathode Pad Chambers (CPC) in the case of μ1 or combinations of CPC's and Multigap Resistive Pad Chambers (MRPC) for μ2, 3 ,4 and 5. Each of the μ1-5 stations consists of two planes of either CPC's or MRPC's made up of a number of individual CPC or MRPC chambers. The inclusion of two planes per station allows for two independent measurements of the muon trajectory in order to obtain good efficiency of the L0 muon trigger and, in the case of the CPCs', is necessary to obtain single crossing timing. The L0 muon trigger, as described below, requires a hit in all five stations resulting in an L0 trigger efficiency which depends on the individual station efficiency as

ϵ^5.

2 Muon Detector Layout

2.1 The Muon Shield

The muon shield is composed of several components including the electromagnetic and hadronic calorimeter and five segments of shielding steel weighing approximately 2,250 tons. The thickness of the shield is constrained by the size of the Delphi experimental area which has been assigned to LHCb. Table 1 below gives the thicknesses of the shield components and avialable space for the placement of the chambers within the shield.

Shield Element	Composition ($\approx 80\%/20\%$)	ρ g/cm^3	X_o cm	λ_o cm	dE/dx MeV/cm	Length m	Length GeV	Length z/X_o	Length λ_o
EM Cal.	Pb/Scint.	4.47	1.64	39.8	8.06	0.50	0.40	30.5	1.26
Had Cal.	Fe/Scint.	6.07	2.55	22.5	12.36	1.50	1.85	58.8	6.67
Shield-0	Fe	7.80	1.78	19.2	15.50	0.30	0.468	16.8	1.56
μ_2 Chamber						0.40			
Shield-1	Fe	7.80	1.78	19.2	15.50	0.70	1.08	39.3	3.65
μ_3 Chamber						0.40			
Shield-2	Fe	7.80	1.78	19.2	15.50	0.70	1.08	39.3	3.65
μ_4 Chamber						0.40			
Shield-3	Fe	7.80	1.78	19.2	15.50	0.70	1.08	39.3	3.65
μ_5 Chamber						0.40			

Table 1: Muon Detector Components

2.2 The Muon Stations

The muon stations μ1-5 are positioned as shown in Fig. 1 and listed in Table 1. The four muon stations, $\mu 2 - \mu 5$, are embedded in the muon shield at average positions of 15.50, 16.60, 17.70 and 18.80 meters respectively relative to the center of the interaction region. The muon stations embedded in the steel have approximately 40 cm of space along the beam available for installation. The remaining station, μ1, is positioned at 12.15 meters from the target, immediately in front of the electromagnetic detector. Each station consists of two "planes" of muon chambers which provide for two independent measurements of the x,y position of penetrating muon from each station. The stations inside the steel are protected from the beam by shielding between the steel walls which extends from 10 mrad to 12 mrad.

2.3 The Muon Chamber Pad Structure

The necessity of forming the Level 0 muon trigger in 3.2 μs has resulted in a decision to incorporate a 2D pad structure in $\mu 1 - 5$ so that muon 3D hit information is available at the earliest possible time for the Level 0 muon trigger. In order to minimize the number of pads required, each of the five muon stations shown in Fig. 1 is composed of four regions with different pad sizes. The pad sizes in each muon plane increase by a factor of 2 as we proceed from the region nearest the beam to the outermost region, thereby approximately preserving the average solid angle subtended by a pad in the different regions. The pad sizes in a given station are scaled relative to the upstream most muon station $\mu 1$ by the relative z position of the given station save for the exceptions noted below.

The x and y sizes of the pads in μ stations 1 and 2 are dictated by the precision which the x projection trajectory of the muon must be measured in order to obtain good resolution on muon p_t for the Level 0 trigger and rejection of spurious machine associated backgrounds [2] by pointing at the interaction region in the y projection. Since more precision is required in the bend plane (x) to determine the muon p_t than in the non-bend plane (y), an y/x aspect ratio = 2 has been adopted for the μ1-2 pads.

The sizes in μ 3, 4 and 5 are set by the requirements of clean pattern recognition of penetrating muons and formation of triple coincidence seeds for finding the muon hits in $\mu 1$ and 2. After studies of pad sizes based on the effect on pattern recognition and Level 0 trigger performance, the pad structure given in Table 2 and shown in Fig. 2 below has been adopted for $\mu 1$. The pad configuration of $\mu 2$ is exactly the same except the pad sizes have been scaled by the ratio of the z positions of $\mu 1$ and 2 to make the pad configuration of $\mu 1$ and 2 projective in both the x and y projections to the interaction region.

The pad configuration for μ 3, 4 and 5 follows a similar pattern except that the x pad size in μ3-5 has been doubled relative to the x pad sizes of $\mu 1$ and 2, reflecting the lesser requirement of spatial resolution required to find the triple coincidences. Hence, μ3, 4 and 5 pads have y/x aspect ratios of 1/1 but are still projective to the interaction region.

Region	x (cm)	y (cm)	θ_x (mrad)	θ_y (mrad)	Pad Size (cm)	# of pads
Beam Hole	$\mid x \mid \leq 30$	$\mid y \mid \leq 18$	$\mid \theta_x \mid \leq 24.7$	$\mid \theta_y \mid \leq 14.8$	-	-
I	$\mid x \mid \leq 40$	$\mid y \mid \leq 32$	$\mid \theta_x \mid \leq 34.6$	$\mid \theta_y \mid \leq 26.3$	1.0x2.0	1480
II	$\mid x \mid \leq 128$	$\mid y \mid \leq 96$	$\mid \theta_x \mid \leq 105.3$	$\mid \theta_y \mid \leq 79.0$	2.0x4.0	5504
III	$\mid x \mid \leq 240$	$\mid y \mid \leq 176$	$\mid \theta_x \mid \leq 197.5$	$\mid \theta_y \mid \leq 144.9$	4.0x8.0	3744
IV	$\mid x \mid \leq 368$	$\mid y \mid \leq 304$	$\mid \theta_x \mid \leq 302.9$	$\mid \theta_y \mid \leq 250.2$	8.0x16.0	2176

Table 2: $\mu 1$ plane pad structure; each nested inner region is excluded from the next larger region

With this choice of pad structure, each $\mu 1$ and $\mu 2$ plane has 12,904 pads, and individual μ3, 4 and 5 planes have 6,452 pads each. Since each "station" has two such planes, the numbers of pads in stations $\mu 1$, 2, 3, 4, and 5 are 25,808, 25,808, 12,904, 12,904 and 12,904 respectively for a total of 90,328 pads. Since we plan to OR together corresponding pads in

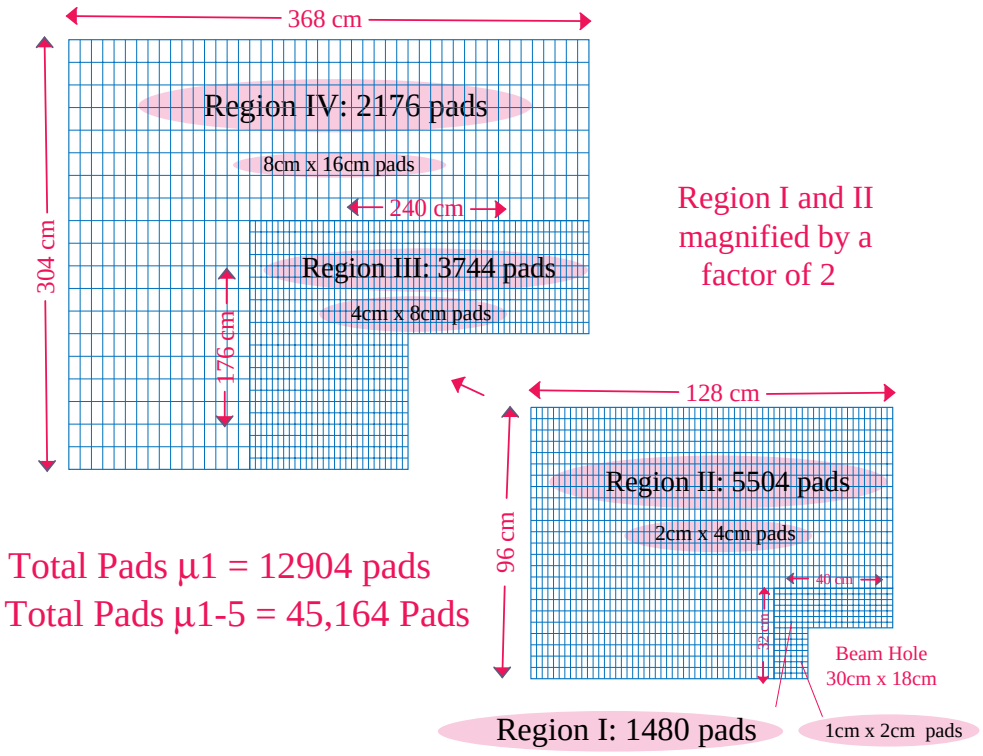

Figure 2: $\mu 1$ pad configuration

the two planes that make up a given station at the periphery of the stations, the number of "logical" pads fed to the L0 trigger processor will be one half this or 45,164.

Given that the pads in the outer regions are quite large, we plan to break up the larger pads into smaller physical pads, each of which will have its individual preamplifer and discriminator. The discriminator outputs for the set of small pads corresponding to a large "logical" pad will be ORed locally at the chamber preserving the 45,164 "logical" channels.

3 The L0 Muon Trigger

The Level 0 muon trigger has a fundamental design goal of reducing the muon trigger rate due to $\pi/K \rightarrow \mu + x$ decays from minimum bias events while maintaining good efficiency for $B \rightarrow \mu + x$.

The present L0 muon trigger algorithm involves the following steps in chronological sequence:

- form triple concidences of $\mu 3$ pad hits with hits found in specified search regions in $\mu 4$ and 5.
- for all such triple coincidences, open search regions in $\mu 2$ based on $\mu 3$ "seed" and form all $\mu 2$-$\mu 3$ combinations.

- calculate x intercepts at $\mu 1$ of $\mu 2$-$\mu 3$ combinations.
- find closest hit pad in $\mu 1$ to x intercept of $\mu 2$-$\mu 3$ projection into $\mu 1$.
- calculate the $\mu 1$-$\mu 2$ combination x and y slopes and y intercept at the interaction region.
- require that the y intercept at z=0 be within a certain distance of the center of the interaction region in the y projection.
- calculate the p_t of the muon candidate from the x slope of the $\mu 1$-$\mu 2$ combination assuming that the track originated in the target and impose a minimum p_t requirement.
- pass on θ_x, θ_y, the x and y intercept at $\mu 1$, the y intercept at the interaction region and the trigger p_t to the Level 1 trigger.

These steps must be performed in less than 3.2 μs to be consistent with the length of the Level 0 pipeline. Like the the hadron and electron Level 0 triggers, the Level 0 muon trigger requires the determination of the p_t of the candidate muons. Unlike the hadron and electron Level 0 triggers, which rely on the electromagnetic and hadronic calorimetery for determination of the energy of the electrons and hadrons, and, thus, the p_t, the Level 0 muon trigger requires the determination of the trajectory of muon in order to ascertain the the momentum and, therefore, the p_t of the muon candidates from their magnetic bending. Fig. 3 shows the resolution of the muon trigger p_t.

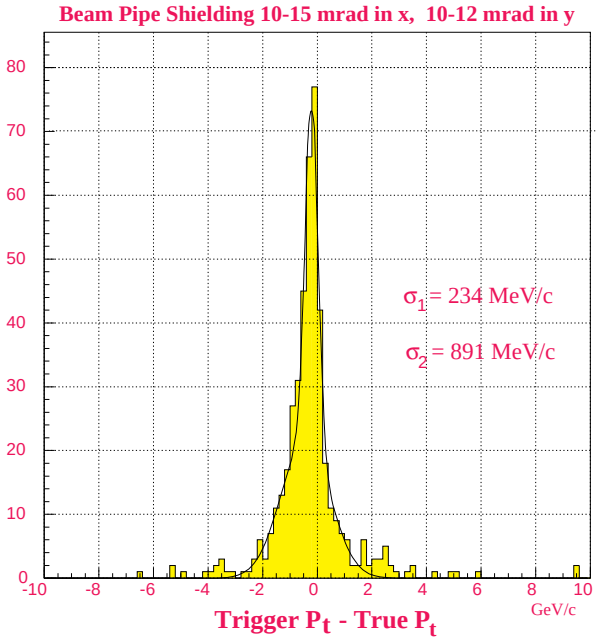

Figure 3: Muon trigger p_t minus true p_t for $B \rightarrow \mu$

3.1 L0 Muon Trigger Studies

Many studies [1] have been performed to determine the sensitivity of the Level 0 trigger rates and efficiencies to various aspects of the LHCb spectrometer and muon system. Among the studies performed were studies to determine the effect of

- varying geometric acceptance of the L0 muon trigger on $B \rightarrow \mu$ efficiencies and minimum bias trigger rates.
- increasing the magnitude of the B_x and B_z magnetic field components.
- various shielding configurations.
- different hadronic shower generation techniques.
- machine associated backgrounds [2].
- different pad sizes and configurations.

We describe below some of the salient results of these studies even though, in some cases, the studies were done with different pad structures, detector placement and, even, different algorithms. In quoting results of studies done with other than the present LHCb muon detector and L0 trigger conditions, we, in general, restrict ourselves to situtations in which can quote relative changes in trigger efficiencies or rates. While the results may be different in detail for the present LHCb trigger conditions, we believe the general conclusions are still valid.

3.1.1 Muon Detector Geometric Acceptance

The determination of the θ_x and θ_y inner and outer angular acceptances of the muon detector geometric acceptance required the simultaneous study of the variation with inner and outer acceptances of

- the rates experienced by the muon stations chambers,
- the $B \rightarrow \mu$ efficiency,
- the minimum bias trigger rate due to $\pi/K \rightarrow \mu$ decays.

A balance of these three features of the muon detector determined the choice of 25 mrad x 15 mrad and 300 mrad x 250 mrad for the inner and outer angular acceptances respectively.

Rates in the Muon Stations

The chamber technology used in given muon stations is determined to a large extent by the rates that must be withstood by the detectors of the μ1-5 stations. The worst case is the μ1 station which is not protected by the shield. The μ2-5 stations in the shield are

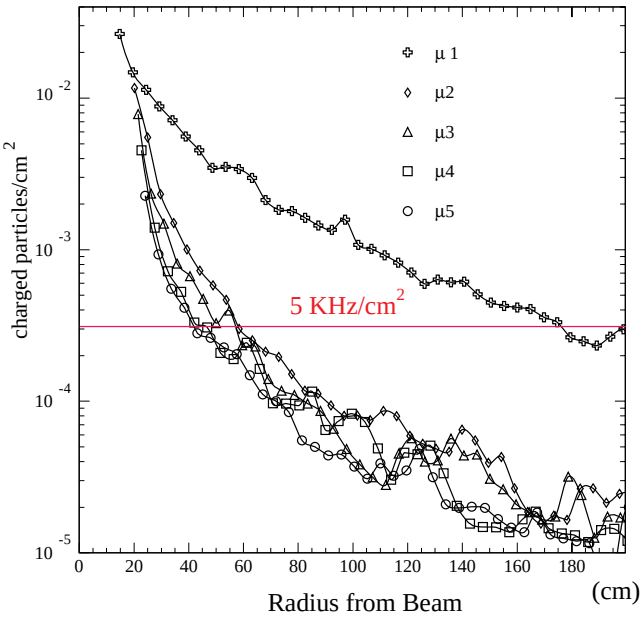

Figure 4: Muon plane μ1-5 rates per cm^2 per interaction as a function of distance from the beam

relatively quiet with, as expected, the upstream-most chamber μ2 being the worst case. However, as shown by Fig. 4, the μ2-5 rates, as estimated using the MARS shower program, in most regions are less than 5 KHz/cm^2 at the average anticipated LHCb luminosity of $L = 2 \times 10^{32} cm^{-2} s^{-1}$. We indicate in Fig. 4 where the 5 KHz/cm^2 limit would occur in μ1-5.

The 25 mrad x 15 mrad inner aperture is approximately consistent with the closest positioning in y that that can be achieved for the active area of the detectors allowing for edge effects in the chambers and the 10-12 mrad shielding from the beam.

We plan, at present, to use a mixture of Multigap Resistive Plate Chambers [3, 4] and Cathode Pad Chambers (CPC's) [5] [6] in the Muon Detector. Which technologies are used in what stations and and what part of the angular coverage is still under study. The details of where the boundaries lie between where one must invoke the CPC technology which is presumably able to handle higher rates and MRPC's which have an as yet unknown rate limitation, will depend on more source and beam testing of prototypes. At present, 5 KHz/cm^2 represents a "flood illumination" limit at which Multigap Resistive Plate Detector (MRPC) efficiencies begin to be unacceptable ($\leq$98%). However, early "spot illumination" tests suggest that much higher rates can be withstood by MRPC's. The CPC's, which are more expensive, should be able to withstand the rates everywhere in μ1-5. While exact coverages are yet to be determined, it can be concluded at this point that a large fraction of the coverage of μ1 must be provided by CPC's and most of the coverage of μ2-5 can be provided by MRPC's.

Variation of Trigger Rates and $B \rightarrow \mu$ Efficiencies with Aperture

In addition to considering the limits on aperture imposed by the rate considerations and the physical extent of the chambers and shielding, we have evaluated the loss of $B \rightarrow \mu$ efficiency and decrease of minimum bias trigger rate caused by increasing the minimum inner acceptance angle. We have also tuned the outer acceptance by studying the variation of the $B \rightarrow \mu$ efficiency and the minimum bias trigger rate as we change the outer acceptance.

We show Fig. 5a the variation of minimum bias retention as the inner acceptance angle is varied (for this study, only θ_x is varied; θ_y is held constant at 15 mrad and the outer angular acceptance was set to 300 mrad x 250 mrad). The baseline inner acceptance of the LHCb Muon Detector of 25 mrad x 15 mrad is indicated by the arrow. The trigger rate at the base line inner acceptance has dropped by 10% relative to an inner angular acceptance of 18 mrad x 15 mrad (taken to be 100% for purposes of Fig. 5)

The variation of minimum bias trigger rate as a function of outer acceptance angle relative to an acceptance of 300 mrad x 300 mrad (where the outer acceptance is taken to be symmetric in θ_x and θ_y for all points *except* the baseline outer acceptance of 300 mrad x 250 mrad of the LHCb Muon Detector) is shown in Fig. 5b. For this study, the inner acceptance was set to 18 mrad x 15 mrad the baseline acceptance point, 300 x 250 mrad, is plotted at 275 mrad, the average of the θ_x and θ_y acceptance.

The comparable plots for variation of $B \rightarrow \mu$ efficiency vs inner and outer acceptance angles are shown in Figs. 6a and b. One of the conclusions that can be drawn from comparing the $B \rightarrow \mu$ efficiency and minimum bias retention plots for inner and outer acceptance variations, is that elimination of the θ_x angular region between 18 mrad and 25 mrad lowers the trigger rate by 5% and the $B \rightarrow \mu$ efficiency by 5%. Therefore, the loss of efficiency can be compensated for by adjusting the p_t cut of the L0 trigger. To the contrary, decreasing the outer acceptance angles causes a greater loss $B \rightarrow \mu$ efficiency than decrease of trigger rate, reflecting the larger p_t of muons from $B \rightarrow \mu$ decays relative to muons from minimum bias events. It is therefore desirable to maintain a 300 mrad x 250 mrad outer acceptance. As can be seen, going beyond 300 mrad gains very little at the expense of a much larger muon detector.

3.1.2 Effect of Different Muon Shielding Configurations on L0 Trigger Rates

Several different muon shielding studies have been performed in an attempt to find an optimal shielding configuration to reduce the effect on muon L0 trigger rates of showering of secondaries from the 14 TeV pp interactions with the beam pipe inside the muon shield. We have compared minimum bias trigger rates with a shield that extends from 4 mrad to 12 mrad (the point at which the frames of the muon detector begin) with a much more modest shield that extends 10 mrad to 12 mrad. The comparison of minimum bias retention as a function of trigger p_t is shown in Fig. 7. Near $p_t \approx 1.0$ GeV/c, the nominal L0 trigger setting, there is very little difference in min bias retention for the two shielding configurations. At lower and higher p_t, the 4-12 mrad shielding is somewhat better. However, the difficulties of access to the beam pipe for baking and the greater restriction on pumping speed for the smaller beam pipe of the 4-12 mrad shielding configuration argues in favor of the 10-12

mrad configuration.

3.1.3 Effect of B_x and B_z on the L0 Trigger Rates

Since the L0 trigger requires construction of the muon trajectory and reconstruction of muon momentum and p_t in 3.2μs, a time constraint which precludes any detailed tracking of the muon trajectory through a non-uniform magnetic field, it is important to estimate the effect of magnetic field non-uniformities on trigger rates and efficiencies. To do this, we used the magnetic field map of the LHCb magnet as a baseline and increased the size of the non-major magnetic field components, B_x and B_z, by factors of 2 and 4 to see the effect on trigger rates and $B \to \mu$ efficiency. The changes relative to the actual magnetic

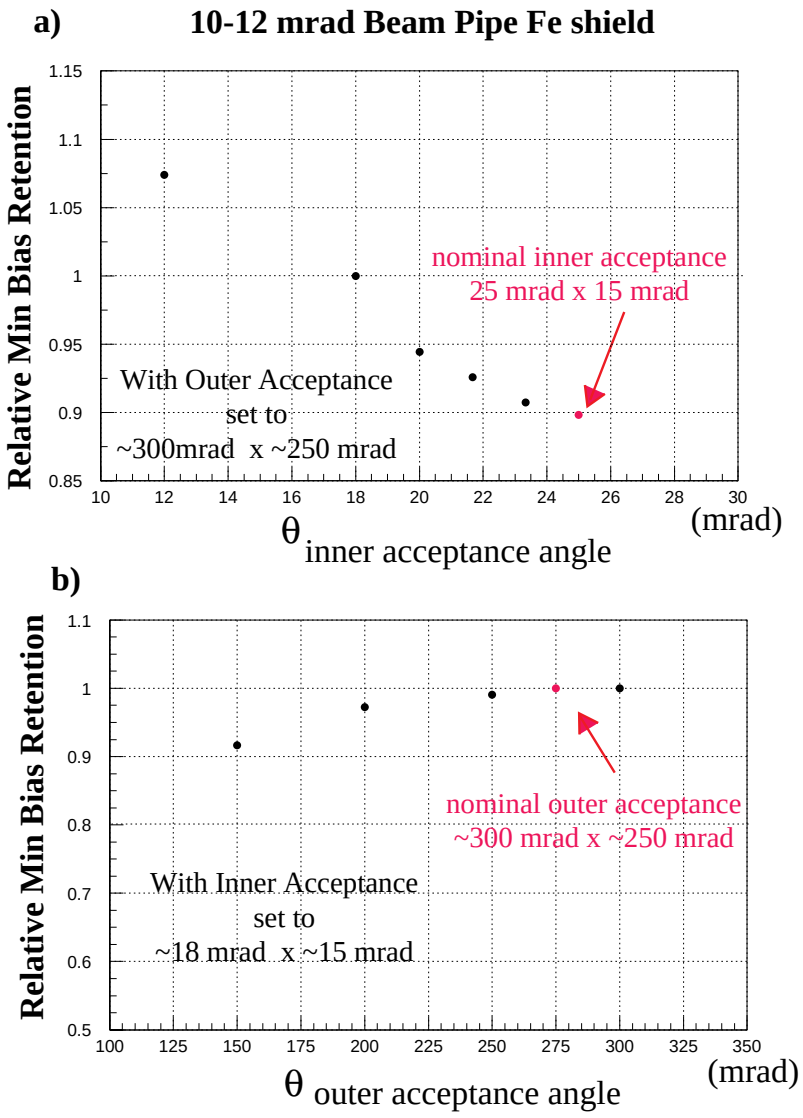

Figure 5: Variation of minimum bias L0 muon trigger rates with inner and outer aperture

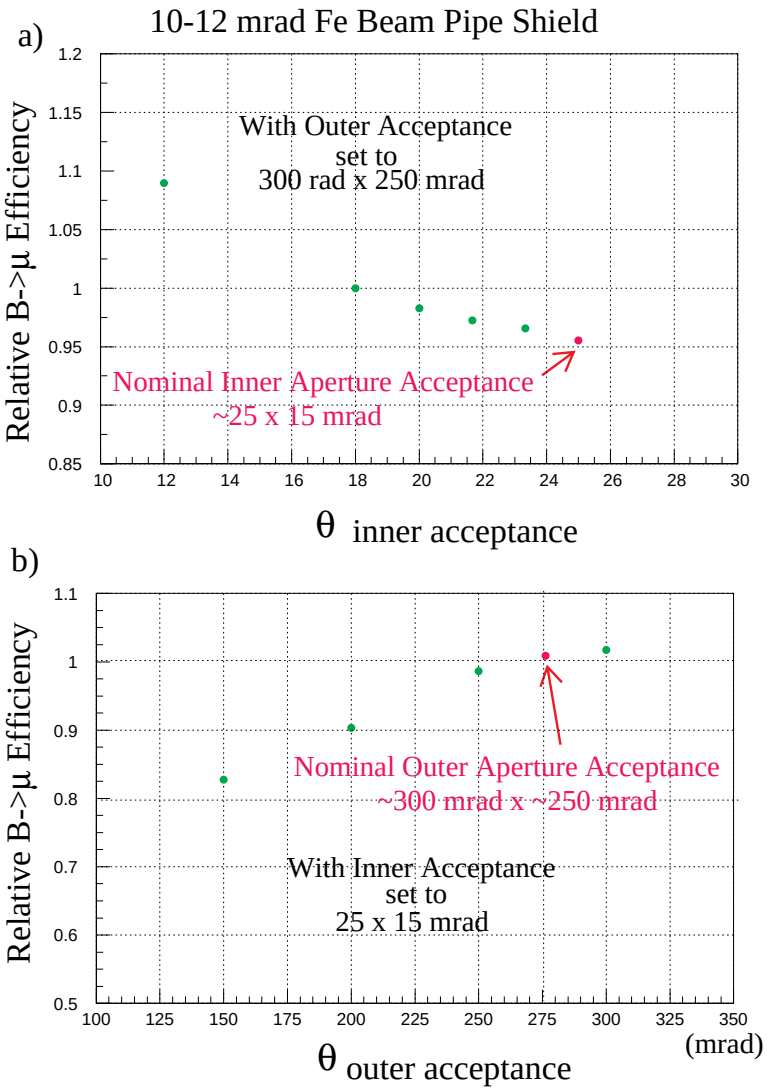

Figure 6: Variation of $B \rightarrow \mu$ efficiency with inner and outer aperture

field map of the LHCb magnet are shown in Fig. 8.

As can be seen, the $B \rightarrow \mu$ efficiency shows practically no change with increased magnetic field non-uniformity. However, the minimum bias trigger retention shows a significant increase, indicating a need to maintain good field uniformity, insofar as possible, in the LHCb magnet. This study was done with an earlier version of the L0 trigger algorithm, the LHCb LOI pad structure, and larger inner acceptance than is presently contemplated so the conclusions may be quantitatively changed if the study were to be repeated.

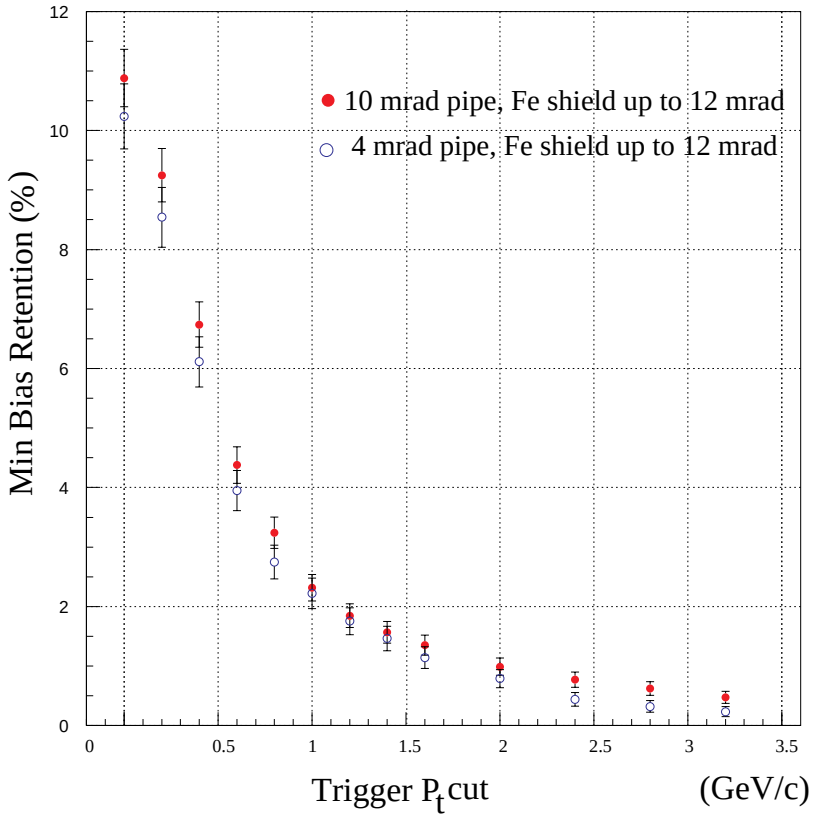

Figure 7: Comparison of L0 muon trigger rates for 4-12 mrad shielding vs. 10-12 mrad shielding configuration around beam pipe in Muon Detector

3.2 L0 Muon Trigger Rates

While small effects on trigger rates and $B \rightarrow \mu$ efficiencies were uncovered in our studies described above, they have either been corrected by changes in design of the muon detector, muon station pad structure or L0 trigger algorithm, or were ignored because they were small. The trigger rates given below were calculated with as realistic a simulation of the LHCb spectrometer using the complete field map for the LHCb analysis magnet and full shower generation in the muon shield (with charged hadrons, electrons, photons, and neutrons tracked down to 1 Mev). The 10-12 mrad shielding configuration between the steel shield walls has been used in obtaining these estimates. The most recent spectrometer muon detector geometry and pad configuration have been used.

The Level 0 muon trigger described above may be tuned by varying the required muon p_t to be relatively "loose" ($\geq$0.7 GeV/c) retaining $\approx$3.0% minimum bias events corresponding to an output Level 0 muon trigger rate of $\approx$300 KHz at the average LHCb luminosity of $2.0\text{x}10^{32}\text{cm}^{-2}\text{s}^{-1}$ (interaction rate of $\approx$16MHz) and an efficiency for $B \rightarrow \mu + X$ in the muon detector acceptance of $\approx$50% for $B \rightarrow \mu$ decays where the muon is pointing to the active area of the Muon Detector. Alternatively, the tune of Level 0 can be tightened ($\geq$1.6 GeV/c) resulting in a minimum bias retention of $\leq$1% with a B efficiency of $\approx$28.0%. Fig. 9 shows the correlation of the minimum bias retention and the B$\rightarrow \mu$ efficiency for the Level 0 muon trigger as well as the for the $B \rightarrow J/\Psi\ \text{K}^0_s$ where the $J/\Psi \rightarrow \mu\mu$. Moreover, for

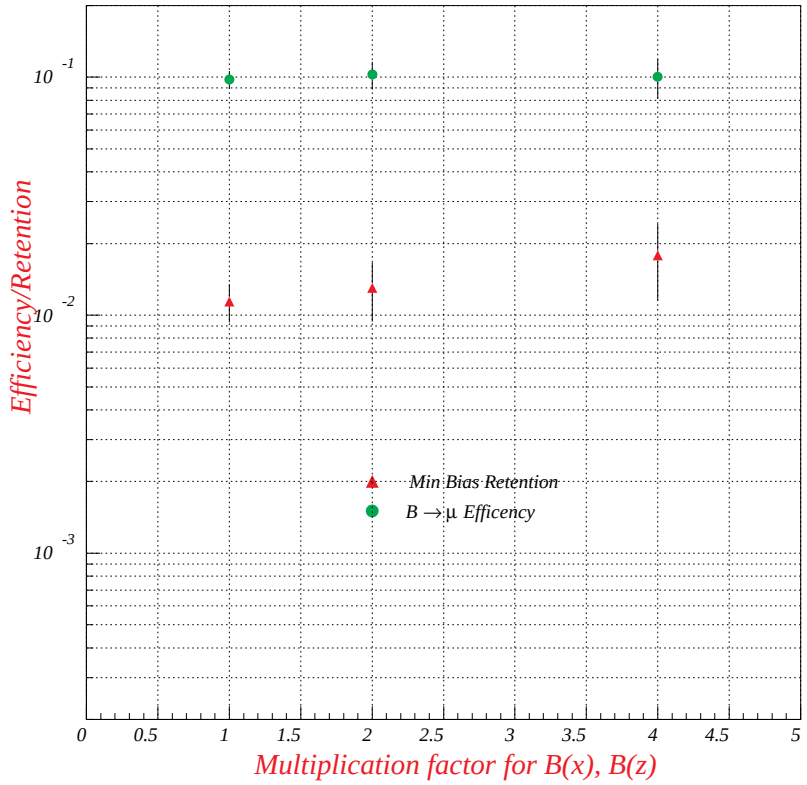

Figure 8: Variation of $B \rightarrow \mu$ efficiency and min bias trigger rate with increasing B_x and B_z

the $B \rightarrow J/\Psi$ K^0_s decay, the B has been reconstructed offline.

4 Conclusions

The Level 0 muon trigger has been studied extensively and has proved to be relatively stable against small variations of strategy and implementaion details of the Level 0 trigger. The trigger algorithm is relatively simple and, because of the pad structure built into the muon planes, can be executed in the requisite 3.2μs, maintaining good efficiency for $B \rightarrow \mu$ decays and good rejection of muons from $\pi/K \rightarrow \mu$ decays in minimum bias events. In addition the trigger is "tunable" so that by varying the required muon p_t the input rate requirements of Level 1 trigger can be met. The hardware implementation of this trigger is discussed elsewhere [7].

We wish to acknowledge the contributions of A.P. McManus and S. Conetti of the University of Virginia, U. Straumann, University of Heidelberg and G. Von Holtey of CERN to this work.

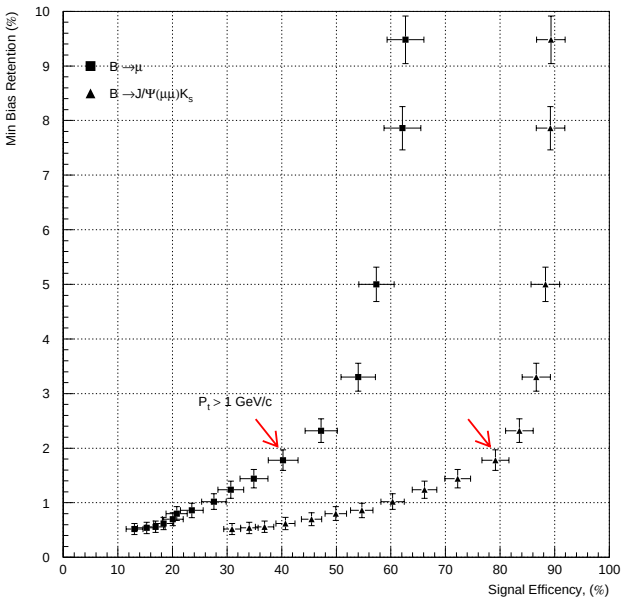

Figure 9: Minimum Bias Retention vs. B$\rightarrow \mu$ and B$\rightarrow J/\Psi \rightarrow \mu\mu$ Efficiencies

References

[1] G. Corti and B. Cox, "The LHCb Muon Trigger", LHCB 97-01 TRIG 97-01, (Jan, 1997); M. Borkovsky, A. Tsaregorodtsev, and A. Vorobyov, "Study of the LHC-B Muon Trigger",(Feb., 1997).

[2] A.I. Droshdin, M. Huhtinen and N.V. Mokhov, "Accelerator Related Background at the CMS Detector at the LHC", CERN CMS TN/96-056, (April, 1996).

[3] E. Cerron Zeballos *et al.*, "A New Type of Resistive Plate Chamber: The Multigap RPC", CERN PPE/95-166, (Nov., 1995); E. Cerron Zeballos *et al.*," Avalanche Fluctuations Within the Multigap Resistive Plate Chamber", CERN/LAA 96-08, (March, 1996).

[4] E. Cerron Zeballos *et al.*, "Pure Avalanche Mode Operation of a 2mm Gap Resistive Plate Chamber", CERN/LAA-MC 97-01, (March, 1997); E. Cerron Zeballos *et al.*, "Micro-streamers and the Micro-gap Resistive Plate Chamber", 4th International RPC Conference, Naples, Italy (Oct., 1997).

[5] LHC-B Letter of Intent, CERN/LHCC/95-5, LHCC/I8 (25 Aug.,95)65.

[6] H. Faissler *et al.*, CERN/DRC/93-49, RD5 Status Report, (1994)25; GEM Technical Design Report, GEM-TN-93-262, SSCL CR, 1219; CMS Technical Proposal, CERN/LHCC/94-38.

[7] G. Corti, B. Cox, and D. Crosseto, K. Nelson, "A Implementation of the LHCb L0 Muon Trigger Using the 3D-Flow ASIC", LHCB 98-001 TRIG/MUON.